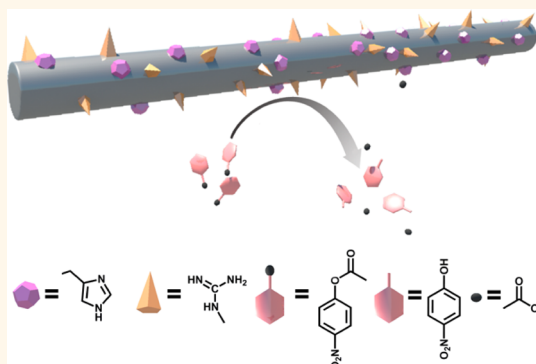# Self-Assembled Peptide Nanofibers Designed as Biological Enzymes for Catalyzing Ester Hydrolysis

Chunqiu Zhang,[†] Xiangdong Xue,[†] Quan Luo,[‡] Yiwei Li,[†] Keni Yang,[†] Xiaoxi Zhuang,[†] Yonggang Jiang,[†] Jinchao Zhang,[§] Junqiu Liu,*,[‡] Guozhang Zou,*,[†] and Xing-Jie Liang*,[†]

[†]CAS Key Laboratory for Biological Effects of Nanomaterials & Nanosafety, National Center for Nanoscience and Technology, No. 11 Beiyitiao, Zhongguancun, Beijing 100190, China, [‡]State Key Laboratory of Supramolecular Structure and Materials, College of Chemistry, Jilin University, Changchun 130012, China, and [§]Chemical Biology Key Laboratory of Hebei Province, College of Chemistry & Environmental Science, Hebei University, Baoding 071002, China

ABSTRACT The structural arrangement of amino acid residues in a native enzyme provides a blueprint for the design of artificial enzymes. One challenge of mimicking the catalytic center of a native enzyme is how to arrange the essential amino acid residues in an appropriate position. In this study, we designed an artificial hydrolase *via* self-assembly of short peptides to catalyze ester hydrolysis. When the assembled hydrolase catalytic sites were embedded in a matrix of peptide nanofibers, they exhibited much higher catalytic efficiency than the peptide nanofibers without the catalytic sites, suggesting that this well-ordered nanostructure is an attractive scaffold for developing new artificial enzymes. Furthermore, the cytotoxicity of the assembled hydrolase was evaluated with human cells, and the novel artificial biological enzyme showed excellent biocompatibility.

Natural enzymes exhibit remarkable catalytic efficiency and substrate specificity due to their unique three-dimensional structures. The amino acid residues fold into precise positions that form the active sites for substrate binding and catalytic reaction. The length of genetically coded protein sequences and the complexity of the folding process create tremendous challenges for fabricating artificial enzymes. In the past decades, much effort has been dedicated to achieve various artificial enzymes,[1−5] and a variety of scaffolds, such as inorganic nanoparticles,[6−8] dendrimers,[9] micelles,[10] nanofibers,[11,12] and nanotubes,[13−15] have been employed to simulate the performance of enzymes. The unique three-dimensional structures built from the nanostructures, similar to proteins, are responsible for high catalytic activities. These successful efforts have provided us with insights about how to incorporate structural and functional features into nanoscaffolds to construct artificial enzymes of high catalytic efficiency.

Among the methods for creating artificial enzymes, the self-assembly approach is more attractive and more similar to protein folding. Natural enzymes fold into their active conformation and gain catalytic activity by self-assembly, and they bind substrates at the catalysis centers mainly *via* noncovalent interactions. This similarity prompted us to fabricate artificial enzymes using self-assembly peptide amphiphiles, polymers, or other organic molecules. Since the major building blocks of peptide amphiphiles are amino acid residues and the driving forces for self-assembly are noncovalent interactions, which share some of the characteristics of natural enzymes, peptide-based nanostructures are the most promising platform for mimicking natural enzymes.[16] Previously, peptide amphiphiles have been employed to self-assemble into nanofibers with catalytic characteristics.[17,18] These peptide amphiphiles are constructed by capping peptides with alkyl chains or other aromatic molecules, which make the
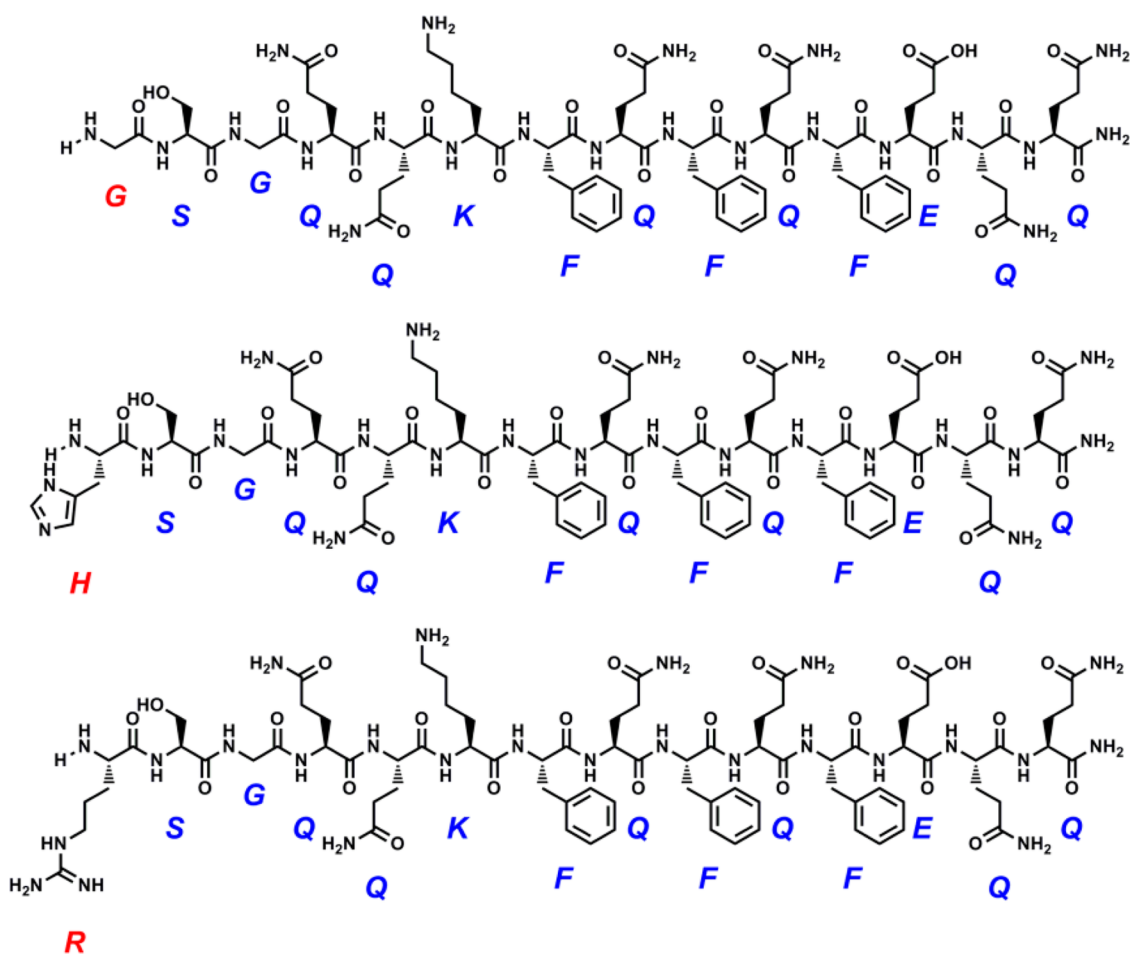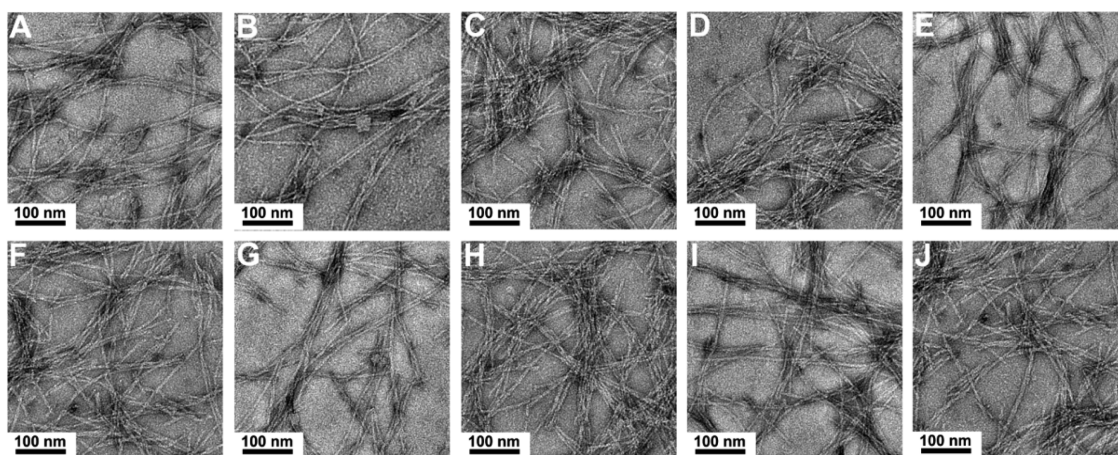
Figure 1. Chemical structures of the peptides used to create hydrolysis models.

peptides amphiphilic to self-assemble into three-dimensional structures. Herein, we seek to use only natural amino acids as building blocks to develop artificial enzymes based on self-assembly of short peptides.

Recently, self-assembly peptide nanofibers with alternating apolar and polar residues were employed for biological applications, such as tissue engineering scaffolds,[19−21] drug release matrices,[22] and platforms for presenting antigen epitopes.[23−25] These self-assembly peptides tend to form β-sheets and subsequently assemble into fibrillar nanostructures.[26−30] In this study, we constructed a hydrolysis module by introducing catalysis centers and binding sites on the surface of self-assembly peptide nanofibers. As the concentration increased, the peptide nanofibers entangled to form a fibrous network, which yielded a hydrogel with hydrolysis activity.

Considering the fact that the imidazolyl groups of histidine residues are essential and are positioned at the catalytic sites of several natural hydrolytic enzymes including trypsin,[31] chymotrypsin,[32] kidney dialkylfluorophosphatase,[33] and so on, some small molecular compounds[34−36] and polymers[37,38] containing imidazole were synthesized and used for the hydrolysis of esters. However, the structures of these artificial enzymes were awry from natural enzymes because the building blocks are not the amino acids. Alternatively, a peptide amphiphilic nanotube with hydrolysis efficacy was fabricated to mimic the structures of natural enzymes.[39] Nevertheless, the structures were susceptible to alteration when adjusting the ratio of histidine to arginine to optimize this model; in some case, the nanotube was damaged. So the structure was not very stable, unlike natural enzymes. Thus, we turned to synthesize a histidine-containing self-assembly peptide Q11H (NH_2-HSGQQKFQFQFEQQ-Am) (as shown in Figure 1). The self-assembly section (QQKFQFQFEQQ) was named Q11. The dipeptide SG was incorporated between H and Q11 as a flexible linker. Q11 was chosen as the scaffold because it was salt-responsive and able to self-assemble into a β-sheet fibrillar nanostructure under mild conditions.[40,41] More importantly, the addition of other amino acids to its termini does not influence the formation of fibrils,[40] so it is possible to put special residues on its surface and arrange the functional residues to achieve certain properties. Furthermore, the Q11 peptide nanofibers were found to be biocompatible and minimally immunogenic.[40] As a control, Q11G

Figure 2. TEM images of a series of the assembled peptide nanofibers. (A) Q11G nanofibers; (B) Q11H nanofibers; (C) Q11R/H = 1/20 nanofibers; (D) Q11R/H = 1/15 nanofibers; (E) Q11R/H = 1/10 nanofibers; (F) Q11R/H = 1/2 nanofibers; (G) Q11R/H = 1/1 nanofibers; (H) Q11R/H = 2/1 nanofibers; (I) Q11R/H = 10/1 nanofibers; (J) Q11R nanofibers.

(NH$_2$-GSGQQKFQFQFEQQ-Am) (as shown in Figure 1) was also synthesized to verify that the Q11 section and the SG linker have no hydrolysis activity and to confirm the essential role of the H residue at the hydrolytic center.

The peptide Q11R (NH$_2$-RSGQQKFQFQFEQQ-Am) (as shown in Figure 1) was synthesized because the guanidyl group of the arginine residue is expected to stabilize the transition state of the substrate at the binding site. In light of the synergistic interaction between the catalysis center and substrate binding site of a natural enzyme, Q11R was coassembled with Q11H, the peptide bearing the catalytic residue, in different proportions to facilitate substrate binding. The enzymatic activities of the coassembled Q11H/Q11R peptides were then examined, and an optimized hydrolase enzyme assembly (Q11HR$_{max}$) was determined. Subsequently, transmission electron microscopy (TEM) imaging and CD spectroscopy were exploited to determine the structure of the nanofibers. The fluorescence of thioflavin-T (ThT), a potent fluorescent marker of amyloid fibrils, was also examined. Finally, the activity of the hydrogel enzyme model (Q11HR$_{max}$gel) was tested, and an MTT assay was performed to test its cytotoxicity.
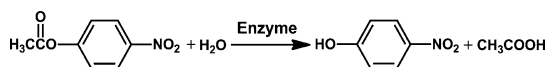
RESULTS AND DISCUSSION

Morphological Characterization of Peptide Nanofibers. Peptide Q11 was found to be soluble and stable in water and formed nanofibers after adding salt, indicating that Q11 is salt-responsive. In this work, we chose Q11 as a scaffold and conjugated an inactive amino acid residue (Gly), a catalytic residue (His), and a binding residue (Arg) with Q11 to obtain peptides Q11G, Q11H, and Q11R, respectively. In order to obtain the optimum hydrolysis model, a series of coassembled peptide nanofibers were prepared with different proportions of peptides Q11H and Q11R. The ratio of R/H ranged from 10/1 to 1/20. To further determine the morphology of these nanofibers, TEM was employed to explore whether the incorporation of other amino acids would affect the basic structure of Q11 nanofibers. As shown in Figure 2, no change was observed in the morphology of the different nanofibers, and the diameter was approximately 10 nm in each case, indicating that the Q11 section was stable and the self-assembly conformation was consistent for all the prepared samples.

Characterization of the Secondary Structure of Peptide Nanofibers. Circular dichroism (CD) spectroscopy and ThT fluorescence spectrum analysis were utilized to evaluate the secondary structures of the peptide nanofibers. As shown in Figure 3A, all examples exhibited negative peaks near 200 nm, indicating a dominant presence of β-sheet conformation, which is consistent with other similar short β-sheet-forming peptides.[42−45] In addition, ThT binding also verified the presence of β-sheets in these fibrillar aggregates.[46] ThT binds to fibrils in preference to monomeric peptides, and the binding can be conveniently determined due to a large enhancement in the fluorescence of this dye (Figure 3B). Indeed, all of the samples tended to have very strong fluorescence enhancement in this assay, indicative of extended amyloid-like fibrils.

Catalytic Activity of Peptide Nanofibers. The hydrolysis of phenyl acetate was monitored by measuring production of the hydrolytic product 4-nitrophenol, which shows increased absorption at 400 nm. The catalytic reaction equation is as follows:

$$H_3CCO\text{—}\langle\bigcirc\rangle\text{—}NO_2 + H_2O \xrightarrow{\text{Enzyme}} HO\text{—}\langle\bigcirc\rangle\text{—}NO_2 + CH_3COOH$$

The hydrolysis of phenyl acetate was previously reported to be first-order with respect to the imidazole concentration.[47] The imidazole directly reacts with the phenyl acetate to form phenol and acylium ionimidazole complexes. The complex then reacts with water to form acetic acid and imidazole. We first tested the
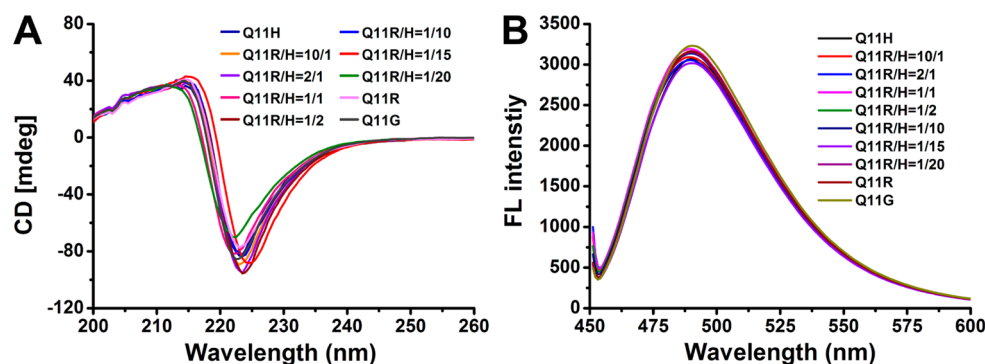
Figure 3. Characterization of the secondary structure of peptide nanofibers. (A) Circular dichroism of a series of coassembled peptide nanofibers in a dilute solution (100 μM). (B) Fluorescence spectra of ThT in the presence of peptide nanofibers (100 μM) (λ_{ex} = 440 nm).
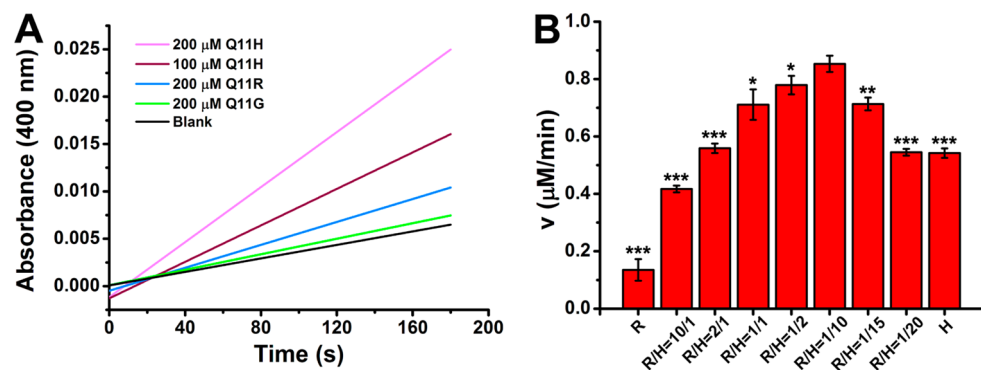

Figure 4. (A) Plots of absorbance *vs* time for hydrolysis of PNPA (0.5 mM). (B) Catalytic reaction rates for hydrolysis of PNPA (0.5 mM) *vs* molar ratio of Q11R to Q11H. $0.01 < *P < 0.05$, $0.001 < **P < 0.01$, and $***P < 0.001$ *vs* Q11R/H = 1/10. The concentration of the Q11 section was fixed at 200 μM.

control peptide Q11G (no catalytic residues) and found that the rate of hydrolysis of PNPA by 200 μM Q11G was very slow, similar to the blank reaction (no peptide fibers added) (Figure 4A). Thus, the Q11 backbone section was not able to hydrolyze PNPA. However, the addition of Q11H (100 and 200 μM) resulted in a distinct enhancement of the hydrolytic rate, and the catalytic rate increased in linear proportion to the increase in enzyme concentration (Figure 4A). Furthermore, we also measured the reaction rate of hydrolysis catalyzed by the coassembled peptide nanofibers with varied molar ratio of Q11H and Q11G and found that, with the increasing ratio of Q11H moiety, the hydrolysis rate increased (Supporting Information Figure S4). We believe that the hydrolytic rate enhancement by Q11H nanofibers was due to the presence of a high density of reactive His residues on the surface of the nanostructures, through the imidazolyl group which activates a water molecule.

To enhance the catalytic rate of hydrolysis, a series of coassembled peptide nanofibers was prepared by optimizing the molar ratio between Q11H and Q11R. In this experiment, the combined concentration of Q11R and Q11H was maintained at 200 μM, and only the molar ratio between Q11H and Q11R was varied. The catalytic activities of different coassembled nanofibers

were measured under the same conditions. As shown in Figure 4B, at the initial stage, the incorporation of Q11R actually increased the catalytic rate, and when the ratio of R/H was 1/10, the catalytic rate reached its maximum value. After that, further increases in the ratio of R/H decreased the hydrolytic rate and a very low hydrolytic rate was observed when the peptide nanofibers were composed exclusively of Q11R. Thus, the hydrolytic rate was optimal when the molar ratio of Q11R to Q11H was 1/10. The optimal hydrolysis model was named Q11HR$_{max}$.

Determination of the Hydrolysis Kinetic Parameters of the Peptide Nanofibers. To investigate the enzymatic kinetics, the initial rates of hydrolysis of PNPA catalyzed by Q11H and Q11HR$_{max}$ were measured as a function of the substrate concentration by varying the concentration of PNPA while keeping the concentration of enzymes fixed. Double-reciprocal plots of the initial rate *versus* substrate concentration were obtained (Figure 5). According to the Michaelis—Menten equation,[48] the apparent kinetic parameters were calculated (Table 1). The results revealed that Q11HR$_{max}$ exhibited stronger binding affinity for PNPA because the substrate binding constant $K_{mQ11HRmax}$ was lower than that of Q11H. Thus, the hydrolysis enzyme model Q11HR$_{max}$ exhibited an enhanced catalytic rate and a higher second-order constant, due to the
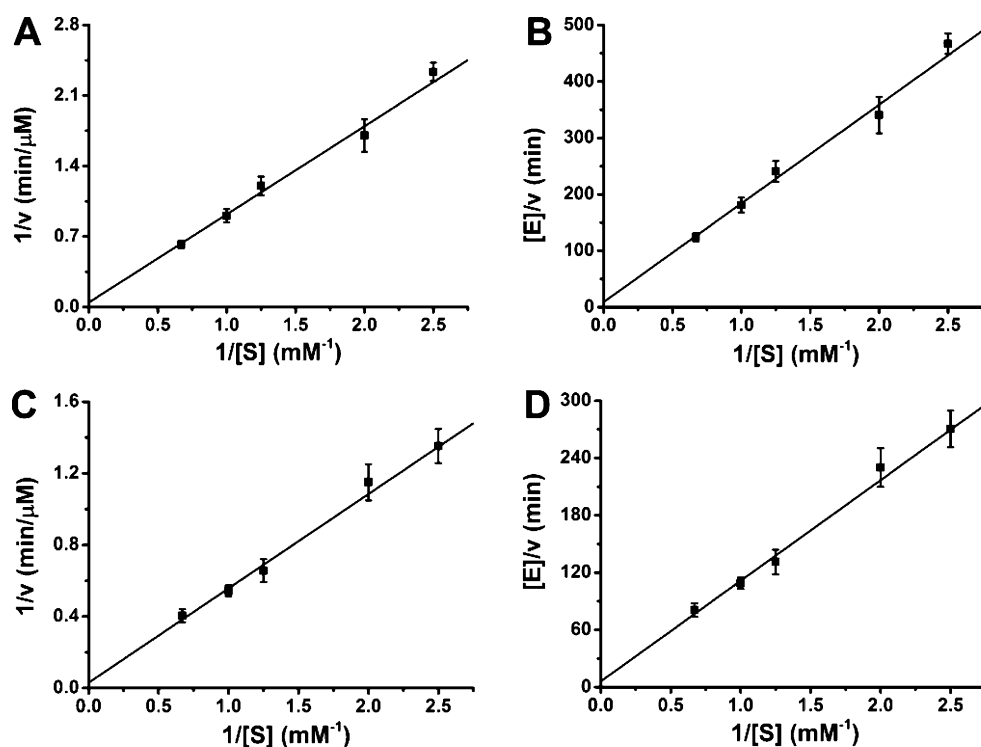
Figure 5. (A,B) Lineweaver−Burk plots of PNPA hydrolysis catalyzed by Q11H ($[E_0] = 200\,\mu$M). (C,D) Lineweaver−Burk plots of PNPA hydrolysis catalyzed by Q11HR$_{max}$ ($[E_0] = 200\,\mu$M).

TABLE 1. Esterase Activity for the Designed Peptide Nanofibers in $1\times$ PBS Buffer (pH 7.4)^a

	k_{cat} ($\times 10^{-3}$ s^{-1})	K_m (mM)	k_{cat}/K_m (M^{-1} s^{-1})
Q11H	1.95	21.68	0.09
Q11HR$_{max}$	2.64	17.63	0.15

^{a} The background of all samples without peptide nanofibers has been subtracted.

incorporation of Arg residues on the surface of the nanofibers as binding sites to stabilize the transition state. Thus, we propose a possible catalytic mechanism for the Q11HR$_{max}$ nanofibers (Figure 6). Initially, the imidazolyl group of the histidine residue activates a H_2O molecule to produce a hydroxide ion, which attacks the carbonyl of PNPA as a nucleophilic moiety to generate a tetrahedral transition state. Then, the guanidyl group of the arginine residue stabilizes the tetrahedral transition state by binding the oxide ions of the tetrahedral intermediate complex and activates the C−O bond for cleavage. Finally, the product p-nitrophenol is released and the next catalysis cycle begins.

Morphological and Catalytic Activity Characterization of the Q11HR$_{max}$ Hydrogel. Since the peptide hydrogel consists of cross-linked nanofiber matrices, which can physically support the active sites and enhance the stability of the nanofibers, we further constructed a hydrogel hydrolysis model by increasing the concentration Q11HR$_{max}$ fibers in water to form a hydrogel (Figure 7A). The mechanical property of the Q11HR$_{max}$ hydrogel (0.5 wt %) was tested by rheology. In the linear

viscoelastic region, the values of the dynamic storage moduli (G') were larger than the dynamic loss moduli (G''), which indicated the formation of a typical soft solid-like gel-phase material (Figure 7B,C). In addition, the morphology of the hydrogel was investigated by TEM. As shown in Figure 7D, networks of nanofibers were observed and the fibers entangled with each other to form a 3D network. This model was able to hydrolyze PNPA in its hydrogel state, similar to the performance of Q11HR$_{max}$ nanofibers (Figure 7E).

Cytotoxicity Study of Peptide Nanofibers. The cytotoxicity of Q11G, Q11H, Q11R, and Q11HR$_{max}$ nanofibers was evaluated using MTT assays. As shown in Figure S5, after incubating cells with Q11G, Q11H, Q11R, or Q11HR$_{max}$ nanofibers at equal concentrations (0.5−100 μM) for 24 h, only a slight decrease in cell viability was observed for each sample. The results suggest that the peptide nanofibers had low toxicity and good biocompatibility.

CONCLUSION

In this study, short peptides were designed to form amyloid-like nanofibers for efficient catalysis of ester hydrolysis. The strategy to display multiple functional residues on the surface of nanofibers provides unlimited opportunities for constructing artificial enzymes by simply coassembling peptides with different active residues. This approach is a promising method for developing hydrogels to mimic natural enzymes. It is also possible to achieve multienzyme systems by
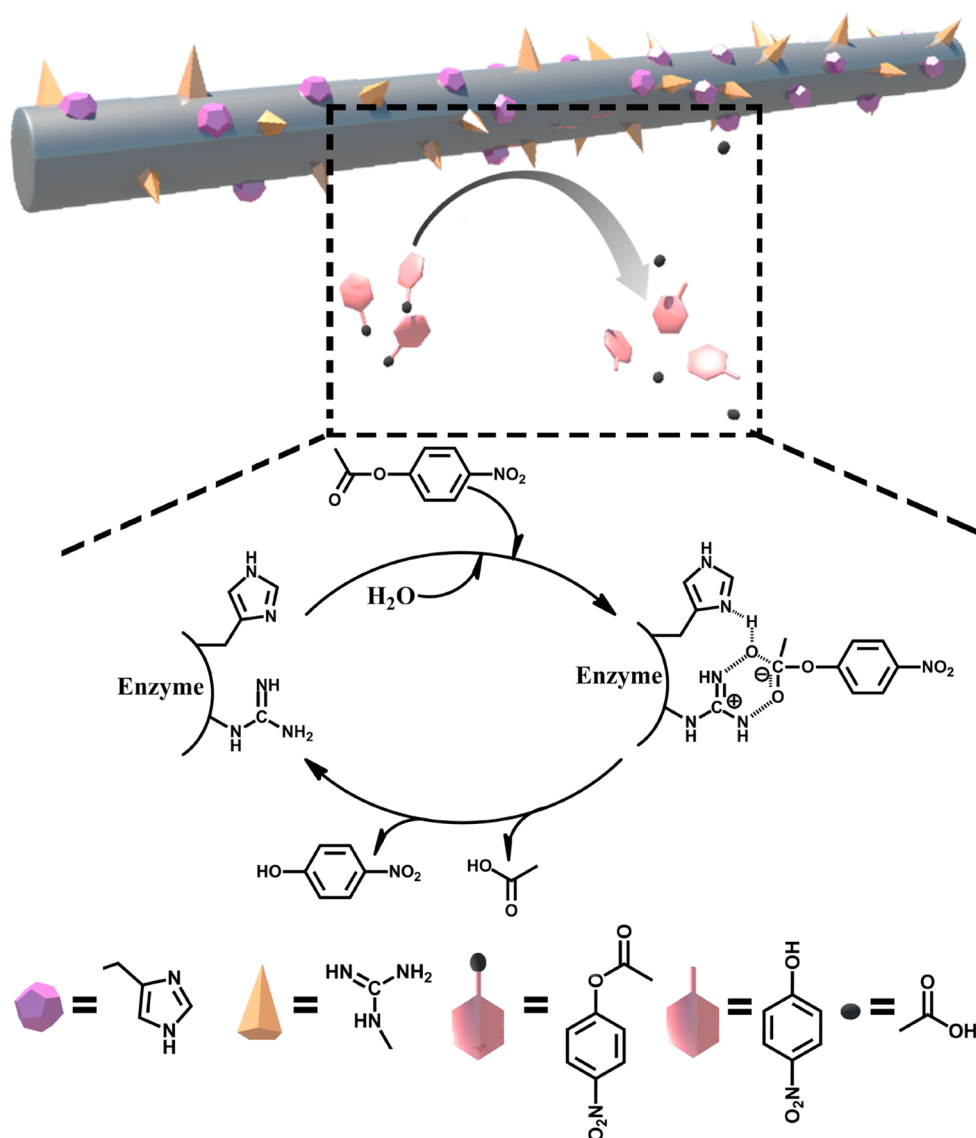
Figure 6. Schematic representation of possible mechanisms for the cleavage of PNPA catalyzed by Q11HR$_{max}$ nanofibers.

mixing other enzymes in the hydrogel. Further use and development of artificial enzymes will guide our

understanding of the synergies between different enzymes and will promote practical applications.
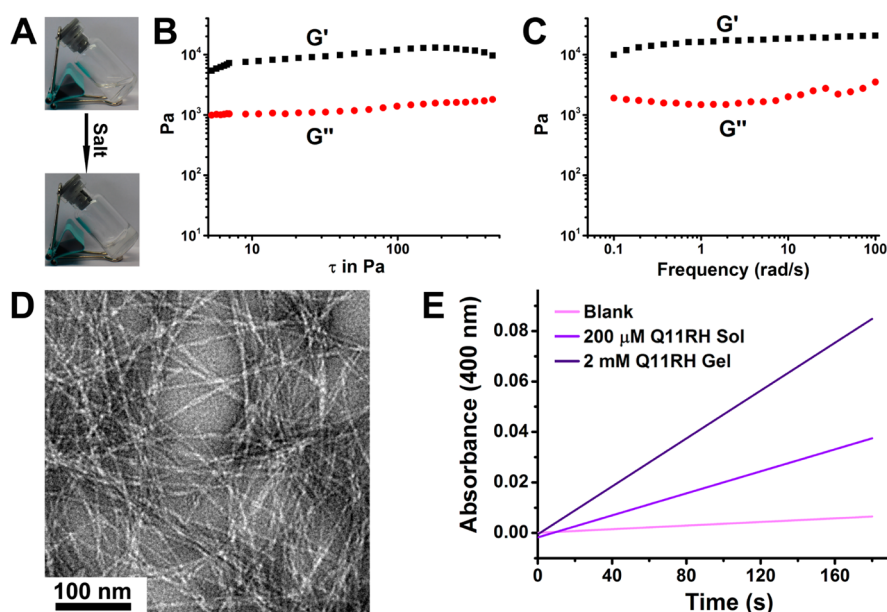
EXPERIMENTAL SECTION

Materials. Fmoc amino acids, diisopropylethylamine (DIEA), and O-(7-azabenzotriazole-1-yl)-1,1,3,3-tetramethyluronilum hexafluorophosphate (HATU) were purchased from BO MAI JIE Technology Co., Ltd. (Beijing, China). The other chemicals and solvents were purchased from Alfa or HEOWNS and used as provided

Peptide Synthesis. Q11G, Q11H, and Q11R peptides were constructed by standard Fmoc solid-phase peptide synthesis on CLEAR amide resin. First, resins were swelled in anhydrous N,N'-dimethylformamide (DMF) for 30 min and then treated with 20% piperidine for Fmoc removal. The first Fmoc-protected amino acid was coupled to the amino groups on the resins using HATU and DIEA as the coupling reagent in DMF. After reacting for 30 min, the mixture was filtered and the resins were washed by dichloromethane and DMF for three times. Next, 20% piperidine in DMF was used for Fmoc removal, and then amino acid couplings were performed using HATU and DIEA as the

coupling reagent as previously described. After the last coupling step, cleavage of the peptides from the resin was performed using a mixture of TFA, 1,2-ethanedithiol, thioanisole, and anisole for 3 h at room temperature. The mixture was then precipitated by ice-cold diethyl ether. The resulting precipitates were washed by ice-cold diethyl ether and dissolved in acetonitrile for HPLC purification. The purified products were characterized by HPLC and MALDI-TOF-MS (Figures S1–S3).

Characterization of Q11G, Q11H, and Q11R by HPLC and MALDI-TOF-MS. The purified peptide Q11G, Q11H, or Q11R was analyzed using RP-HPLC on a C18 column. Elution was monitored with a diode array detector at wavelength of 214 nm. Peptide Q11G, Q11H, or Q11R was eluted with a linear gradient at the flow rate of 1 mL/min. The elution solvent consisted of solvent A (water with 0.1% TFA) and solvent B (acetonitrile with 0.1% TFA). A linear gradient of 5 to 95% solvent B over 45 min was used. The purified peptide molecular weight of Q11G, Q11H, or Q11R was confirmed by MALDI-TOF-MS using a Microflex LRF System

Figure 7. (A) Photographic images of the transformation from solution to hydrogel of peptide Q11HR$_{max}$ (0.5 wt %). (B) Dynamic storage modulus (G') and loss modulus (G'') vs strain for Q11HR$_{max}$ hydrogel (0.5 wt %). (C) Frequency dependence of dynamic storage modulus (G') and loss modulus (G'') of Q11HR$_{max}$ hydrogel (0.5 wt %). (D) TEM image of Q11HR$_{max}$ nanofibers in the hydrogel. (E) Plots of absorbance vs time for hydrolysis of PNPA (0.5 mM).

spectrometer (Bruker Daltonics). One microliter of peptide solution was spotted onto a 100-well MALDI plate and dried at room temperature. Then, another 1 μL solution (saturated α-cyano-4-hydroxycinnamic acid dissolved in 1:1 acetonitrile/H$_2$O with 0.1% TFA) was spotted on the dried peptide spot. The samples were analyzed in positive reflector mode.

Preparation of Self-Assembly Peptide Nanofibers Q11G and Q11H. Q11G or Q11H peptide powder was dissolved in 900 μL of deionized water at a concentration of 4.44 mM at room temperature. Then, 100 μL of 10× PBS buffer (pH 7.4) was added into the peptide solution to obtain a peptide hydrogel (4 mM) after storing for 24 h at room temperature. Before the activity was tested, the hydrogel was diluted 1:9 in 1× PBS buffer (9 mL) and vortexed vigorously to disrupt the gel-like self-assembled structure to obtain nanofiber solution at a final peptide concentration of 400 μM.

Preparation of Coassembly Peptide Nanofiber Q11HG. Different molar ratios of peptides Q11H and Q11G were mixed in 900 μL of deionized water at a fixed combined concentration of 4.44 mM of the Q11 section. A series of coassembly peptide nanofibers was prepared by adding 100 μL of 10× PBS buffer (pH 7.4) into the peptide solutions and then storing for 24 h at room temperature for forming the hydrogels (4 mM). Before the activity was tested, the hydrogels were diluted 1:9 in 1× PBS (9 mL) and vortexed vigorously to disrupt the gel-like self-assembled structures to obtain nanofiber solutions at a final peptide concentration of 400 μM.

Preparation of Coassembly Peptide Nanofiber Q11HR. Different molar ratios of peptides Q11H and Q11R were mixed in 900 μL of deionized water at a fixed combined concentration of 4.44 mM of the Q11 section. A series of coassembly peptide nanofibers was prepared by adding 100 μL of 10× PBS buffer (pH 7.4) into the peptide solutions and then storing for 24 h at room temperature for forming the hydrogels (4 mM). Before the activity was tested, the hydrogels were diluted 1:9 in 1× PBS (9 mL) and vortexed vigorously to disrupt the gel-like self-assembled structure to obtain nanofiber solutions at a final peptide concentration of 400 μM.

Circular Dichroism Spectroscopy. A J-810-CD spectropolarimeter (JASCO, Japan) was used to collect CD spectra in 1× PBS buffer (pH 7.4) at 100 μM concentration of the Q11 section with a 1 cm quartz cell. The measurements were performed from 200 to 280 nm with a scan speed of 100 nm/min, 1 nm step resolution, and 3 accumulations at room temperature.

Thioflavin-T Fluorescence. Fluorescence spectra of thioflavin-T were measured using a fluorescence spectrophotometer (HITACHI F-4600). Nanofiber solutions at 100 μM of each peptide were incubated with 1 mM thioflavin-T for 10 min, and the emission spectrum was recorded with the excitation at 440 nm.

Transmission Electron Microscopy Characterization. The TEM samples were prepared from 10 μM nanofiber solutions on a carbon-coated copper grid (from Zhongjingkeyi Technology Co. Ltd., Beijing, China). A 4 μL droplet of the nanofiber solution was dropped on the copper grid and placed at room temperature overnight for drying. A 4 μL droplet of 1% uranyl acetate solution was then added, and staining was allowed to proceed for 1.5 min, followed by removal of excess solution. The grid was washed by deionized water three times and left covered under a Petri dish to dry. TEM micrographs were collected on a Tecnai G2 20 S-TWIN transmission electron microscope with 200 kV acceleration voltage.

Determination of the Catalytic Activity of p-Nitrophenyl Acetate Hydrolysis. The catalytic activities of the prepared samples were determined using p-nitrophenyl acetate (PNPA) as the substrate. The hydrolytic product was 4-nitrophenol with an absorption peak at 400 nm, so the reaction rate was determined by monitoring the absorbance at 400 nm with a LABTECH UV Bluestar A1301124 spectrophotometer. PNPA hydrolysis was done in a quartz cuvette containing 200 μL of 1× PBS buffer, 500 μM PNPA, and a certain amount of catalyst.

Kinetics Experiments. The kinetics experiments were performed as described above. PNPA hydrolysis was done in a quartz cuvette containing 200 μL of 1× PBS buffer, a series of PNPA concentrations, and 200 μM catalyst. The rate constants were calculated by the Michaelis–Menten equation.

Rheology. A HAAKE MARS system was used for rheology test. The aqueous solution containing the gelator was directly dropped onto 20 mm parallel plates, then PBS solution was added into the solution, which was incubated for 10 min. After a stable hydrogel had formed, the linear viscoelastic region and frequency dependence of dynamic storage modulus (G') and loss modulus (G'') of the hydrogel were determined by the mode of dynamic frequency sweep in the region of 0.1–100 rad/s.

Cell Culture. Human normal hepatocyte cell line L02 was maintained in Dulbecco's modified Eagle's medium/high glucose with 10% fetal bovine serum in a humidified atmosphere containing 5% CO$_2$ at 37 °C.

MTT Assay. L02 cells were seeded in 96-well plates at an intensity of 4×10^3 cells per well. After 24 h incubation, the medium were replaced by Q11G, Q11H, Q11R, or Q11HR$_{max}$ nanofiber solution at Q11 section concentration ranging from 0.5 to 100 μM for 24 h at 37 °C. Then, the medium in each well was replaced by 100 μL of 0.5 mg/mL MTT solution, and after 3 h incubation, the MTT solution was removed and 150 μL DMSO per well was added. The absorbance of MTT at 570 nm was measured by an Infinite M200 microplate reader (Tecan, Durbam, USA) with a reference wavelength of 630 nm. Cell viability was calculated by the ratio of the absorbance of the nanofibers treated cells to that of untreated cells in culture medium.

Conflict of Interest: The authors declare no competing financial interest.

Supporting Information Available: Additional figures. This material is available free of charge *via* the Internet at http://pubs.acs.org.

REFERENCES AND NOTES

1. Breslow, R.; Dong, S. D. Biomimetic Reactions Catalyzed by Cyclodextrins and Their Derivatives. *Chem. Rev.* **1998**, *98*, 1997–2012.
2. Kirby, A. J. Enzyme Mechanisms, Models, and Mimics. *Angew. Chem., Int. Ed. Engl.* **1996**, *35*, 706–724.
3. Qi, D.; Tann, C. M.; Haring, D.; Distefano, M. D. Generation of New Enzymes *via* Covalent Modification of Existing Proteins. *Chem. Rev.* **2001**, *101*, 3081–3111.
4. Murakami, Y.; Kikuchi, J. J.; Hisaeda, Y.; Hayashida, O. Artificial Enzymes. *Chem. Rev.* **1996**, *96*, 721–758.
5. Wulff, G. Enzyme-like Catalysis by Molecularly Imprinted Polymers. *Chem. Rev.* **2002**, *102*, 1–27.
6. Astruc, D.; Lu, F.; Aranzaes, J. R. Nanoparticles as Recyclable Catalysts: The Frontier between Homogeneous and Heterogeneous Catalysis. *Angew. Chem., Int. Ed.* **2005**, *44*, 7852–7872.
7. Zaramella, D.; Scrimin, P.; Prins, L. J. Self-Assembly of a Catalytic Multivalent Peptide−Nanoparticle Complex. *J. Am. Chem. Soc.* **2012**, *134*, 8396–8399.
8. Lin, Y.; Ren, J.; Qu, X. Nano-Gold as Artificial Enzymes: Hidden Talents. *Adv. Mater.* **2014**, *26*, 4200–4217.
9. Kofoed, J.; Reymond, J. L. Dendrimers as Artificial Enzymes. *Curr. Opin. Chem. Biol.* **2005**, *9*, 656–664.
10. Huang, X.; Dong, Z.; Liu, J.; Mao, S.; Xu, J.; Luo, G.; Shen, J. Selenium-Mediated Micellar Catalyst: An Efficient Enzyme Model for Glutathione Peroxidase-like Catalysis. *Langmuir* **2007**, *23*, 1518–1522.
11. Guler, M. O.; Stupp, S. I. A Self-Assembled Nanofiber Catalyst for Ester Hydrolysis. *J. Am. Chem. Soc.* **2007**, *129*, 12082–12083.
12. Rufo, C. M.; Moroz, Y. S.; Moroz, O. V.; Stohr, J.; Smith, T. A.; Hu, X.; DeGrado, W. F.; Korendovych, I. V. Short Peptides Self-Assemble To Produce Catalytic Amyloids. *Nat. Chem.* **2014**, *6*, 303–309.
13. Tang, Y.; Zhou, L.; Li, J.; Luo, Q.; Huang, X.; Wu, P.; Wang, Y.; Xu, J.; Shen, J.; Liu, J. Giant Nanotubes Loaded with Artificial Peroxidase Centers: Self-Assembly of Supramolecular Amphiphiles as a Tool To Functionalize Nanotubes. *Angew. Chem., Int. Ed.* **2010**, *49*, 3920–3924.
14. Hou, C.; Luo, Q.; Liu, J.; Miao, L.; Zhang, C.; Gao, Y.; Zhang, X.; Xu, J.; Dong, Z.; Liu, J. Construction of GPx Active Centers on Natural Protein Nanodisk/Nanotube: A New Way To Develop Artificial Nanoenzyme. *ACS Nano* **2012**, *6*, 8692–8701.
15. Huang, X.; Liu, X.; Luo, Q.; Liu, J.; Shen, J. Artificial Seleno-enzymes: Designed and Redesigned. *Chem. Soc. Rev.* **2011**, *40*, 1171–1184.
16. Gao, Y.; Zhao, F.; Wang, Q.; Zhang, Y.; Xu, B. Small Peptide Nanofibers as the Matrices of Molecular Hydrogels for Mimicking Enzymes and Enhancing the Activity of Enzymes. *Chem. Soc. Rev.* **2010**, *39*, 3425–3433.
17. Rodriguez-Llansola, F.; Miravet, J. F.; Escuder, B. A Supramolecular Hydrogel as a Reusable Heterogeneous Catalyst for the Direct Aldol Reaction. *Chem. Commun.* **2009**, 7303–7305.
18. Terech, P.; Weiss, R. G. Low Molecular Mass Gelators of Organic Liquids and the Properties of Their Gels. *Chem. Rev.* **1997**, *97*, 3133–3160.
19. Jung, J. P.; Nagaraj, A. K.; Fox, E. K.; Rudra, J. S.; Devgun, J. M.; Collier, J. H. Co-assembling Peptides as Defined Matrices for Endothelial Cells. *Biomaterials* **2009**, *30*, 2400–2410.
20. Collier, J. H. Modular Self-Assembling Biomaterials for Directing Cellular Responses. *Soft Matter* **2008**, *4*, 2310–2315.
21. Aggeli, A.; Bell, M.; Boden, N.; Keen, J. N.; Knowles, P. F.; McLeish, T. C.; Pitkeathly, M.; Radford, S. E. Responsive Gels Formed by the Spontaneous Self-Assembly of Peptides into Polymeric β-Sheet Tapes. *Nature* **1997**, *386*, 259–262.
22. Altunbas, A.; Lee, S. J.; Rajasekaran, S. A.; Schneider, J. P.; Pochan, D. J. Encapsulation of Curcumin in Self-Assembling Peptide Hydrogels as Injectable Drug Delivery Vehicles. *Biomaterials* **2011**, *32*, 5906–5914.
23. Rudra, J. S.; Tian, Y. F.; Jung, J. P.; Collier, J. H. A Self-Assembling Peptide Acting as an Immune Adjuvant. *Proc. Natl. Acad. Sci. U.S.A.* **2010**, *107*, 622–627.
24. Huang, Z. H.; Shi, L.; Ma, J. W.; Sun, Z. Y.; Cai, H.; Chen, Y. X.; Zhao, Y. F.; Li, Y. M. A Totally Synthetic, Self-Assembling, Adjuvant-Free MUC1 Glycopeptide Vaccine for Cancer Therapy. *J. Am. Chem. Soc.* **2012**, *134*, 8730–8733.
25. Rudra, J. S.; Sun, T.; Bird, K. C.; Daniels, M. D.; Gasiorowski, J. Z.; Chong, A. S.; Collier, J. H. Modulating Adaptive Immune Responses to Peptide Self-Assemblies. *ACS Nano* **2012**, *6*, 1557–1564.
26. Collier, J. H.; Hu, B. H.; Ruberti, J. W.; Zhang, J.; Shum, P.; Thompson, D. H.; Messersmith, P. B. Thermally and Photochemically Triggered Self-Assembly of Peptide Hydrogels. *J. Am. Chem. Soc.* **2001**, *123*, 9463–9464.
27. Aggeli, A.; Bell, M.; Boden, N.; Keen, J. N.; Knowles, P. F.; McLeish, T. C.; Pitkeathly, M.; Radford, S. E. Responsive Gels Formed by the Spontaneous Self-Assembly of Peptides into Polymeric β-Sheet Tapes. *Nature* **1997**, *386*, 259–262.
28. Schneider, J. P.; Pochan, D. J.; Ozbas, B.; Rajagopal, K.; Pakstis, L.; Kretsinger, J. Responsive Hydrogels from the Intramolecular Folding and Self-Assembly of a Designed Peptide. *J. Am. Chem. Soc.* **2002**, *124*, 15030–15037.
29. Zhang, S.; Holmes, T.; Lockshin, C.; Rich, A. Spontaneous Assembly of a Self-Complementary Oligopeptide To Form a Stable Macroscopic Membrane. *Proc. Natl. Acad. Sci. U.S.A.* **1993**, *90*, 3334–3338.
30. Lashuel, H. A.; Labrenz, S. R.; Woo, L.; Serpell, L. C.; Kelly, J. W. Protofilaments, Filaments, Ribbons, and Fibrils from Peptidomimetic Self-Assembly: Implications for Amyloid Fibril Formation and Materials Science. *J. Am. Chem. Soc.* **2000**, *122*, 5262–5277.
31. El'skaia, A. V.; Soldatkin, A. P. The Basis of High-Fidelity Translation. *Mol. Biol. (Moscow)* **1984**, *18*, 1163–1180.
32. Gutfreund, H.; Sturtevant, J. M. The Mechanism of the Reaction of Chymotrypsin with *p*-Nitrophenyl Acetate. *Biochem. J.* **1956**, *63*, 656–661.
33. Mounter, L. A. Dialkylfluorophosphatase of Kidney. IV. Dissociation Constant of Active Groups. *J. Biol. Chem.* **1956**, *219*, 677–683.
34. Bender, M.; Turnquest, B. The Imidazole-Catalyzed Hydrolysis of *p*-Nitrophenyl Acetate. *J. Am. Chem. Soc.* **1957**, *79*, 1652–1655.
35. Kirsch, J.; Jencks, W. Base Catalysis of Imidazole Catalysis of Ester Hydrolysis. *J. Am. Chem. Soc.* **1964**, *86*, 833–837.
36. Komiyama, M.; Bender, M. Hydrolysis of *p*-Nitrotrifluoroacetanilide Catalyzed by Water and Imidazole. *Bioorg. Chem.* **1978**, *7*, 133–139.

37. Kunitake, T.; Shimada, F.; Aso, C. Imidazole Catalyses in Aqueous Systems. I. Enzyme-like Catalysis in the Hydrolysis of a Phenyl Ester by Imidazole-Containing Copolymers. *J. Am. Chem. Soc.* **1969**, *91*, 2716–2723.

38. Giusti, L.; Medeiros, M.; Ferreira, N. L.; Mora, J.; Fiedler, H. Polymers Containing Imidazole Groups as Nanoreactors for Hydrolysis of Esters. *J. Phys. Org. Chem.* **2014**, *27*, 297–302.

39. Huang, Z.; Guan, S.; Wang, Y.; Shi, G.; Cao, L.; Gao, Y.; Dong, Z.; Xu, J.; Luo, Q.; Liu, J. Self-Assembly of Amphiphilic Peptides into Bio-functionalized Nanotubes: A Novel Hydrolase Model. *J. Mater. Chem. B* **2013**, *1*, 2297–2304.

40. Collier, J. H.; Messersmith, P. B. Enzymatic Modification of Self-Assembled Peptide Structures with Tissue Transglutaminase. *Bioconjugate Chem.* **2003**, *14*, 748–755.

41. Jung, J. P.; Jones, J. L.; Cronier, S. A.; Collier, J. H. Modulating the Mechanical Properties of Self-Assembled Peptide Hydrogels *via* Native Chemical Ligation. *Biomaterials* **2008**, *29*, 2143–2151.

42. Caplan, M. R.; Moore, P. N.; Zhang, S.; Kamm, R. D.; Lauffenburger, D. A. Self-Assembly of a β-Sheet Protein Governed by Relief of Electrostatic Repulsion Relative to van der Waals Attraction. *Biomacromolecules* **2000**, *1*, 627–631.

43. Eisenberg, D.; Jucker, M. The Amyloid State of Proteins in Human Diseases. *Cell* **2012**, *148*, 1188–1203.

44. Colletier, J. P.; Laganowsky, A.; Landau, M.; Zhao, M.; Soriaga, A. B.; Goldschmidt, L.; Flot, D.; Cascio, D.; Sawaya, M. R.; Eisenberg, D. Molecular Basis for Amyloid-β Polymorphism. *Proc. Natl. Acad. Sci. U.S.A.* **2011**, *108*, 16938–16943.

45. Nowick, J. S. Exploring β-Sheet Structure and Interactions with Chemical Model Systems. *Acc. Chem. Res.* **2008**, *41*, 1319–1330.

46. Biancalana, M.; Koide, S. Molecular Mechanism of Thioflavin-T Binding to Amyloid Fibrils. *Biochim. Biophys. Acta* **2010**, *1804*, 1405–1412.

47. Bruice, T. C.; Sturtevant, J. M. Imidazole Catalysis. V. The Intramolecular Participation of the Imidazolyl Group in the Hydrolysis of Some Esters and the Amide of γ-(4-Imidazolyl)-butyric Acid and 4-(2′-Acetoxyethyl)-imidazole. *J. Am. Chem. Soc.* **1959**, *81*, 2860–2870.

48. Faller, L.; Sturtevant, J. M. The Kinetics of the α-Chymotrypsin-Catalyzed Hydrolysis of *p*-Nitrophenyl Acetate in Organic Solvent−Water Mixtures. *J. Biol. Chem.* **1966**, *241*, 4825–4834.